Journal Name

ARTICLE

Enhanced luminescence performance of CaO:Ce^{3+}, Li^{+}, F^{-} phosphor and its phosphor-in-glass based high-power warm LED properties

Jiankun Deng,[a] Haoran Zhang,[a] Xuejie Zhang,[a] Maxim S. Molokeev,[bcd] Jianbei Qiu,[e] Yingliang Liu,*[a] Bingfu Lei,*[a] Li Ma[f] and Xiaojun Wang[f]

Received 00th January 20xx,
Accepted 00th January 20xx

DOI: 10.1039/x0xx00000x

www.rsc.org/

To obtain white light-emitted diodes (wLEDs) with a low correlated color temperature (CCT) and a high color rendering index (CRI), red-emitting is indispensable in their emission spectra. Herein, CaO:Ce^{3+}, Li^{+}, F^{-} yellow phosphors with more red spectral component have been prepared by high temperature solid-state reaction. Compared to F^{-} undoped samples, CaO:Ce^{3+}, Li^{+}, F^{-} has a lower critical doping concentration of Ce^{3+}, and shows stronger luminescence. At the critical concentration, the quantum efficiency of 66.4% and enhanced thermal and chemical stability are obtained in CaO:Ce^{3+}, Li^{+}, F^{-}. Furthermore, CaO:Ce^{3+}, Li^{+}, F^{-}-based phosphor-in-glass (PiG) using the red-emitting glass system with composition of SiO_2-Na_2CO_3-Al_2O_3-CaO:Eu^{3+} as the host material was constructed and used for high-power white LED applications. Such PiG samples with different phosphor doping concentrations can satisfy various light color demands and own higher reliability than CaO:Ce^{3+}, Li^{+}, F^{-} phosphor. An optimal PiG-based wLED exhibits color coordinates of (0.3769, 0.3386), a CCT of 3774 K, a CRI of 82.5 and a LE of 73.1 when the mass ratio of phosphor to glass matrix is 7:50 in PiG. Besides, such PiG-based wLED also shows acceptable color stability under different drive currents. All above results demonstrate that CaO:Ce^{3+}, Li^{+}, F^{-} can be expected to be an potential alternative yellow phosphor for blue light excited PiG based warm wLEDs, especially for high-power ones.

1. Introduction

Phosphor-converted light-emitted diodes (pcLEDs) have become one of the most important applications in solid-state lighting due to the appearance of white LEDs (wLEDs) fabricated through the combination of the InGaN blue LED chip and Ce^{3+}-doped yttrium aluminum garnet (YAG:Ce^{3+}).[1,2] Nevertheless, some shortcomings, including a low correlated color temperature (CCT) and a high color rendering index (CRI), do exist with such outstanding lighting device. For resolution of the above issues, adding the red spectral component in the emission spectra of wLEDs through the supplement of extra red phosphor or substitution of YAG:Ce^{3+} by other yellow-emitting phosphor is the most frequently used method.[3,4] Nowadays, owing to red phosphors with suitable spectral properties being limit, alternative yellow-emitting phosphors (*e.g.* YAG:Ce^{3+} compositional derivatives), which are devoted to the exploration of adjusting their luminescence properties for containing more red emission, have received more attention.[4] In the evolution of this class of yellow-emitting phosphors, ion substitution is the main approach to achieve the desired objectives.[5-9] The development of other novel yellow-emitting phosphors should be increasingly facilitated for the sake of resource conservation and environmental friendliness.

Calcium oxide (CaO) with the characteristics of abundance, low price and non-toxicity has been widely applied in different fields, such as ceramic, glass, and catalyst.[10-12] Moreover, CaO can be doped with various rare earth ions to obtain a series of phosphor-materials with special properties harvesting of photoluminescence, electron degradation, thermoluminescence, long persistence, energy transfer.[13-18] Among CaO-phosphors, Ce^{3+}-doped CaO (CaO:Ce^{3+}) with simple chemical composition, suitable excitation and emission spectra, is a promising yellow-emitting phosphor for blue light excited wLEDs. In addition, the emission spectrum of CaO:Ce^{3+} owns more red spectral component than the commercialized YAG:Ce^{3+} , making it more appropriate for warm-wLEDs. However, low efficient light conversion and weak chemical stability of CaO:Ce^{3+} are the main factors that restrict its feasibility to replace YAG:Ce^{3+}. To date, some studies have been reported on solving these problems. For example, Hao et al. proposed that alkali metal ion (Li^{+} or Na^{+}) co-doping can effectively increase photoluminescence intensity in CaO:Ce^{3+}.[19, 20] Lehmann found that coating a layer of CaF_2 on the surface of CaO:Ce^{3+} particles can slow down the reaction between CaO:Ce^{3+} and atmospheric moisture.[13] In general, researches on CaO:Ce^{3+} phosphor are still relatively few and need more investments.

In recent years, a new class of luminescent materials, namely phosphor-in-glass (PiG), has been developed to use in the application of the color converters required to have higher performances.[21] In the preparation process of such PiG-materials, low-melting inorganic glass powder is chosen to be the encapsulant and translated into glass matrix to coat the traditional phosphors at a low sintering temperature, which makes PiG retain the advantages of glass, such as high thermal conductivity, excellent chemical stability and good plasticity. Because of the glass-like properties, PiG can afford the heat generated from the high-power LED chip or laser excitation in order to keep from altering the yellowing of its body? color and resist the influences of environment, compared to the color converters using silicone as the encapsulant. A few previous studies have also confirmed the importance of PiG for high-power lighting devices. In 2012, Chung et al.[22] pioneered the use of YAG: Ce^{3+}-PiG for high-power wLEDs. Subsequently, not only YAG: Ce^{3+}-PiG, but also other phosphor-PiGs as the color converters have got great development. [23-27] Especially, the researchers have applied PiG to laser illumination lately.[28,29] Thus it can be seen that PiG technology can give phosphors opportunities to be suitable for high-power lighting. Besides as a robust

[a] *Guangdong Provincial Engineering Technology Research Center for Optical Agricultural, College of Materials and Energy, South China Agricultural University, Guangzhou 510642, China.*
[b] *Laboratory of Crystal Physics, Kirensky Institute of Physics,Federal Research Center KSC SB RAS, Krasnoyarsk 660036, Russia.*
[c] *Department of Physics, Far Eastern State Transport University, Khabarovsk 680021, Russia.*
[d] *Siberian Federal University, Krasnoyarsk, 660041, Russia.*
[e] *Faculty of Materials Science and Engineering, Kunming University of Science and Technology, Kunming, 650093, China.*
[f] *Department of Physics, Georgia Southern University, Statesboro, GA 30460, USA.*
† E-mail: tleibf@scau.edu.cn
Electronic Supplementary Information (ESI) available: details of any supplementary information available should be included here. See DOI: 10.1039/x0xx00000x

encapsulant, glass matrix for PiG can emit red light by trivalent ions (*e.g.* Eu^{3+}, Pr^{3+}) doping, improving the optical properties of corresponding white light devices.[30-32]

On the basis of above considerations, there are reasons to believe that PiG technology makes a good accompaniment to CaO:Ce^{3+} phosphor in the respect of the color converters. In this research, Ce^{3+}, Li^+, F^- triply doped CaO (CaO:Ce^{3+}, Li^+, F^-) phosphor with enhanced luminescence and thermal stability was successfully prepared with a high-temperature solid phase method, and the effects of F^- codoping on various properties of CaO:Ce^{3+}, Li^+ were discussed in detail. A series of robust multi-color CaO:Ce^{3+}, Li^+, F^--PiGs were synthesized by combining CaO:Ce^{3+}, Li^+, F^- and the red-emitting glass system with composition of SiO_2-Na_2CO_3-Al_2O_3-CaO:Eu^{3+}, demonstrating great potential for high-power warm wLEDs.

2. Experimental method

2.1 Preparation

The synthesis processes of CaO:*x*Ce^{3+}, *x*Li^+, 4xF^- (*x* = 0.0004, 0.0006, 0.0008, 0.0012, 0.003, 0.005, 0.007, 0.009, 0.011 and 0.013) using high temperature solid-state reaction, were to mix the stoichiometric amounts of the raw materials, including CaO, CeF and LiF, thoroughly, and then heat the mixture in a tube furnace at 5 °C/min to 1400 °C for 6 h in the reduction atmosphere (5% H_2 + 95% N_2). The obtained samples were cool down naturally in the furnace and ground into powder for subsequent tests. The F^- undopd samples of CaO:*y*Ce^{3+}, *y*Li^+, (*y* = 0.003, 0.005, 0.0007, 0.009, 0.011 and 0.013) using CeO_2 and Li_2CO_3 as the cerium and lithium sources, were chosen as the references and prepared under the same conditions. In addition, CaO:*x*Ce^{3+}, *x*Li^+, 4xF^- (*x* = 0.0006) and CaO:*y*Ce^{3+}, *y*Li^+ (*y* = 0.007), which are representative samples, were denoted as COCLF-6 and COCL-7, respectively, in following content for concise expression.

PiG samples with different mass ratios of phosphor to glass matrix (3:50, 5:50, 3:50 and 9:50) were initially prepared by the mixtures of COCLF-6 and precursor glass frit with composition of SiO_2-Na_2CO_3-Al_2O_3-CaO:Eu^{3+} which was developed in our previous work.[32] Then, the mixtures were compressed into cylinder and sintered at 5 °C/min to 680 °C for 0.5 h in air atmosphere**.** The as-obtained PiG plates were cut into the desired size (ϕ 10 mm disk with thickness of 0.5 mm) and optically polished. The corresponding PiG-based wLEDs were fabricated by combination of the PiG samples and 460 nm high-power blue chip**.**

2.2 Characterization

The photoluminescence excitation (PLE) and photoluminescence (PL) spectra were measured by a F-7000 Hitachi fluorescence spectrofluorometer. The decay curves were recorded by the kinetic mode of FSP920 Time Resolved and Steady State Fluorescence Spectrometers (Edinburgh Instruments, England) equipped with a 150 W nF900 flash lamp as the light source. The structure and phase purity of the samples were analyzed by powder X-ray diffraction (XRD), using a Rigaku Ultima-IV X-ray diffractometer with Cu Kα radiation (λ = 0.15406) at 40 kV and 40 mA. Rietveld analysis for the powder diffraction data of samples was performed by using TOPAS 4.2 system. The X-ray photo-electron spectroscopy (XPS) spectra were measured by employing a Kratos AXIS Ultra DLD X-ray photoelectron spectrometer using a monochromatic Al Ka X-ray source. The morphology observations were obtained by the transmission electron microscopy (TEM) and high-resolution transmission electron microscopy (HRTEM) using a JEOL-2010 electron microscope equipped with an energy-dispersive X-ray spectroscopy (EDS) system. The distribution of phosphor sample and PiG sample were performed by an ultrahigh resolution field-emission scanning electron microscope (FEI, Nova NanoSEM 430) and a confocal laser scanning microscope (LSM 710, Zeiss), equipped with a 458 nm laser for excitation, respectively. The quantum efficiency (QE) was measured by QY2000 (Tianjin Orient-KOJI Instrument, China). The temperature-dependent PL spectra were measured by an F-4600 fluorescence spectrophotometer combined with a heating apparatus (Oxford Instruments). The electroluminescence (EL) of PiG-based wLEDs and corresponding parameters were measured by FSP920 under 9 V operating voltage with corresponding driving currents. The chemical stability of the samples was examined by exposing them in ambient atmosphere for the time period of 10 days.

3. Results and discussion

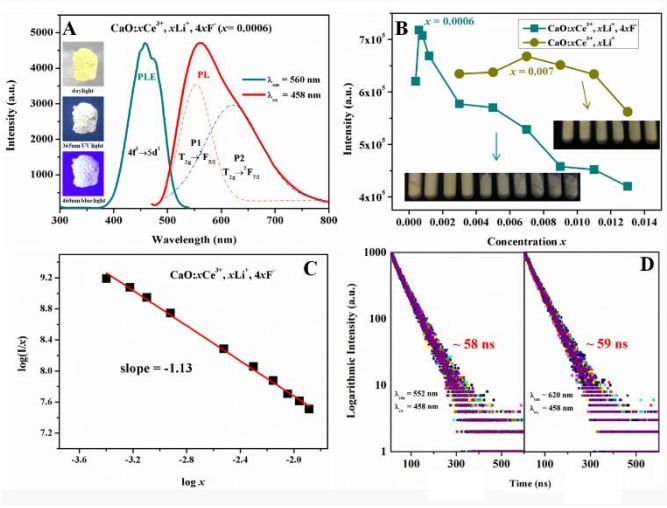

Figure 1. (A) PLE and PL spectra of COCLF-6 phosphor. The insets show photographs of COCLF-6 phosphor in daylight, under 365 nm UV light and 460 nm blue light excitation, respectively. (B) Dependence of emission intensity *versus* *x* in CaO:*x*Ce^{3+}, *x*Li^+, 4xF^- (bluish-green line) and CaO:*y*Ce^{3+}, *y*Li^+ (yellow line), excited at 458 nm. Insets are photographs of corresponding samples with various doping concentration *x* in daylight. (C) log(*I*/*x*) as a function of doping concentration *x* in CaO:*x*Ce^{3+}, *x*Li^+, 4xF^-. (D) Decay curves of the $T_{2g}\rightarrow{}^2F_{5/2}$ (left) and $T_{2g}\rightarrow{}^2F_{7/2}$ (right) transitions for different doping concentrations *x* (0.0004-0.013) in CaO:*x*Ce^{3+}, *x*Li^+, 4xF^-.

Based on the suitable photoluminescence properties, CaO:Ce^{3+}, Li^+, F^- phosphor is a good candidate used for the 460 nm blue light excited wLEDs. The PLE and PL spectra of COCLF-6 are shown in Figure 1A, accompanying with the excitation band located at 458 nm and the emission band around 560 nm. With regard to the former, it is originated from $4f^1\rightarrow5d^1$ transition of Ce^{3+} and almost lacks shorter excitation range (< 350 nm), which can eliminate the effect of the absorption of the glass host when CaO:Ce^{3+}, Li^+, F^- phosphor is applied in PiG-materials. As for the latter, an asymmetric emission broadband is obtained and can be fitted into two Gaussian bands centered at 552 nm (P1, $T_{2g}\rightarrow{}^2F_{5/2}$) and 620 nm (P2, $T_{2g}\rightarrow{}^2F_{7/2}$), respectively. The energy difference between these two Gaussian bands is 1987 cm^{-1}, which is in accordance with the energy gap between $^2F_{5/2}$ and $^2F_{7/2}$. Besides, compared with that of YAG:Ce^{3+}, PL spectrum of COCLF-6 has more required red spectral component for fabrication of wLEDs with high CRI and low CCT (Figure S1). Then, photographs of COCLF-6 phosphor in daylight, under 365 nm UV light and 460 nm blue light excitation, are also illustrated in the inset of Figure 1A. As seen in Figure 1B, the PL intensity reaches a maximum in CaO:Ce^{3+}, Li^+, F^- with the doping concentration of *x* = 0.0006, while the critical concentration of *y* = 0.007 is obtained in CaO:Ce^{3+}, Li^+. Remarkably, the variance between the critical concentrations in such two phosphors is about 10 times, and higher intensity is found in CaO:Ce^{3+}, Li^+, F^-, indicating that F^- ion co-doping exerts important influence on the state of the activator ion (Ce^{3+}) existing in CaO host. In the insets of Figure 1B, F^- doped samples have deeper body color than the undoped ones at the same doping concentration (*x* = 0.003-0.013) of Ce^{3+}, further confirming the above viewpoint. In order to figure out the energy transfer mechanism accounting for concentration quenching, the critical distance (R_c) can be calculated for estimation by the following formula [18, 33]

$$R_c = 2\left(\frac{3V}{4\pi x_c N}\right)^{1/3} \quad (1)$$

where x_c represents the critical doping concentration of Ce^{3+}, while V and N are the unit cell volume of the altered CaO host and the number of unit cell sites occupied by Ce^{3+}, respectively. According to the results of Rietveld structure refinements (Table 1), the values of R_c for COCLF-6 and COCL-7 are 44.6 Å and 19.6 Å. Thus, the types of concentration quenching mechanism of them both belong to multipole–multipole interaction because of inconsistency with others including the exchange interaction ($R_c \approx$ 4 Å) and radiation reabsorption (little overlap between PLE and PL spectra). Moreover, multipole interactions can be subdivided into several types by the Dexter theory, and identified using the following equation [34]

$$I/x = k[1+\beta(x)^{\theta/3}]^{-1} \quad (2)$$

where x and I represent the concentration of Ce^{3+} activator and corresponding PL intensity; k and β are constants for individual interactions in the given matrix; θ can be assigned various values such as 3, 6, 8 or 10, which mean, respectively, the energy migration among nearest neighbor or next nearest neighbor activators, dipole-dipole, dipole-quadrupole, or quadrupole-quadrupole interaction. For calculation of θ, the slope (θ/3) should be firstly obtained from the relationship of log$I$/x with log$x$ by simplifying equation (2). Therefore, the slopes of the fitting lines are -1.13 and -1.05 in Figure 1C and S2, indicating that the concentration quenching behavior occurring in F^- doped and undoped samples are owing to the energy migration among nearest neighbor or next nearest neighbor activators. In other words, F^- doping do not affect the concentration quenching mechanism of CaO:Ce^{3+}, Li^+, but lower its critical quenching concentration, the reason of which may be ascribed to that the environment in which anion (O^{2-}) is located has been changed by the incorporation of F^-, while the one in which cation (Ca^{2+}) is located has not. From Figure 1D, the PL decay curves of the transitions ($T_{2g} \rightarrow {}^2F_{5/2}$ and $T_{2g} \rightarrow {}^2F_{7/2}$) in CaO:$x$$Ce^{3+}$, $x$$Li^+$, 4$x$$F^-$ (x = 0.0004-0.0013) excited at 458 nm and, respectively, monitored at 552 nm and 620 nm are fitted with a single-exponential function, and the lifetime of them can be calculated according to the following equation

$$I = A\exp(\frac{-t}{\tau}) \quad (3)$$

where I represent the PL intensities at the moment of t; A and τ are constant and lifetime, respectively. The values of lifetime for such two transitions are ~58 ns and ~59 ns, which remains almost same while the Ce^{3+} concentration changes. The above results indicate that even through the energy migration among nearest neighbor or next nearest neighbor Ce^{3+} exists, it is with very little influence on the concentration quenching behavior of CaO:Ce^{3+}, Li^+, F^-. Actually, the PL intensity of CaO:Ce^{3+}, Li^+, F^- with different doping concentration should depend on the number of Ce^{3+} absorbing excitation photons.[19,20]

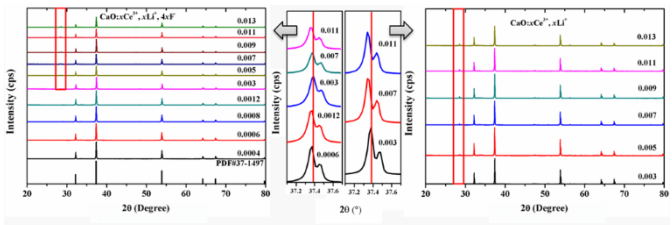

Figure 2. XRD patterns of (A) CaO:$x$$Ce^{3+}$, $x$$Li^+$, 4$x$$F^-$ (x = 0.0004-0.013), standard cubic for CaO (PDF#37-1497), and (B) CaO:$y$$Ce^{3+}$, $y$$Li^+$ (y = 0.003-0.013). (C) The enlarge XRD patterns of corresponding samples from 37.0° to 37.8°. (unify the units, o or degree)

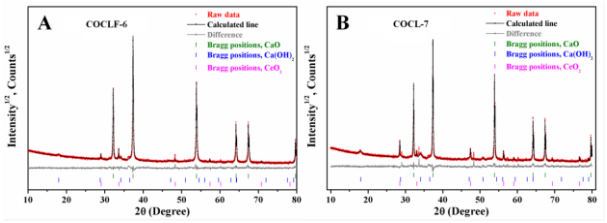

Figure 3. Rietveld refinement analysis of (A) COCLF-6 and (B) COCL-7. Raw data, calculated patterns and the difference between them are presented using red dots, black line and gray line, while Bragg positions of CaO, $Ca(OH)_2$ and CeO_2 are marked with green, blue and pink vertical lines, respectively.

To further understand the role that F^- doping plays in CaO:Ce^{3+}, Li^+ causing the unique optical properties, the structural analysis of CaO:Ce^{3+}, Li^+, F^- and CaO:Ce^{3+}, Li^+ have been studied. The X-ray diffraction (XRD) patterns of CaO:$x$$Ce^{3+}$, $x$$Li^+$, 4$x$$F^-$ (x = 0.0004-0.0013) are given in Figure 2A, showing all obvious characteristic diffraction peaks originated from them almost coincide with those of standard CaO sample (PDF#37-1497), except the one centered at θ = 28.5° belonging to CeO_2 impurity (red rectangle). The similar situation also exists for CaO:$y$$Ce^{3+}$, $y$$Li^+$ (y = 0.003-0.013), as seen in Figure 2B. If the replacement of Ca^{2+} (r = 1 Å) just by Ce^{3+} (r = 1.02 Å) and Li^+ (r = 0.76 Å), the diffraction peaks of CaO host should shift to higher angle because of the radius diversity of the ions ($2r_{Ca^{2+}} > r_{Ce^{3+}} + r_{Li^+}$), however, the phenomenon of which does not appear in CaO:Ce^{3+}, Li^+, F^- and CaO:Ce^{3+}, Li^+ (Figure 2C). More structural information can be obtained from Rietveld refinement analysis of COCLF-6 and COCL-7 performed by using TOPAS 4.2.[35] Almost all peaks are indexed by CaO, $Ca(OH)_2$ and CeO_2 phases.[36-38] Therefore these structures are taken as starting model for Rietveld refinement. Refinements for both samples are stable and give low R-factors (Figure 3 and Table 1). It is worth noting that in addition to CaO and CeO_2, $Ca(OH)_2$ impurity is detected at the same time, and the content of $Ca(OH)_2$ in COCLF-6 is lower than that in COCL-7, implying that a small amount of F^- doping is advantageous to protection of CaO from water infiltration.[13] Meanwhile, the cell volume of both samples are nearly identical, and become bigger contrast to the starting model, which is well agreement with the results of XRD in Figure 2C. Based on the above experimental evidence, the doping mode of Ce (Ce^{3+} and Ce^{4+}) and Li^+ ions in CaO is illustrated in Figure 4A. Inevitably, Ce ions in different states of valence have been maintained during the doping process in consideration of XPS spectra of Ce3d in Figure S3.[39] According to the previous literature reported by Liu et al.,[40] it can be deduced that some Ca^{2+} sites in CaO host lattice are occupied by Ce^{3+} while others are accommodated with Ce^{4+}. The codopant of Li^+ is introduced into interstitial sites as the donor, providing electrons for Ce^{4+}. Thus, not only the cell volume increases but the concentration of activator Ce^{3+} is raised, leading to the enhanced PL intensity of CaO:Ce^{3+}, Li^+. In addition, the cell volume of COCLF-6 ought to be smaller than COCL-7, owing to the lower doping concentration of Ce^{3+} and Li^+ as well as the replacement of O^{2-} by F^- ($r_{O^{2-}} > r_{F^-}$). However, as a matter of fact, the cell volume of the former equals, or even exceeds that of the latter. It may be due to that F^- is successfully doped into CaO host lattice because no phase related to F^- has been found in corresponding XRD patterns, and there is not single but double F^- ions substituting for O^{2-}, keeping the charge balance, so that COCLF-6 has a bigger cell volume (Figure 4B). As for the increase of PL intensity in COCLF-6 compared to COCL-7, we assume that the introduction of F^- would makes the distance between activator Ce^{3+} shorter and results in the decrease of critical quenching concentration of Ce^{3+}, reducing the PL intensity. Nevertheless, the content of $Ca(OH)_2$ impurity in COCLF-6 is also reduced, which is good for the improvement of PL

performance.[20] The comprehensive influence of such two factors above finally determines the optical properties of COCLF-6.

Table 1. Rietveld structure refinement data for COCLF-6 and COCL-7.

Samples	Phase	Space group	Cell parameters (Å)	Cell volume (Å^3)	R_B (%)	R_{wp}, (%)	R_p (%)	χ^2	Content weight (%)
COCLF-6	CaO	*Fm*-3*m*	$a = b = c$ = 4.8087 (5)	V = 111.20 (3)	2.72	9.19	6.27	1.42	93.8 (7)
	$Ca(OH)_2$	*P*-3*m*1	$a = b$ = 3.577 (6) c = 4.918 (9)	V = 54.5 (2)	2.31				5.6 (7)
	CeO_2	*Fm*-3*m*	$a = b = c$ = 5.3214 (2)	V = 150.69 (1)	8.08				0.6 (2)
COCL-7	CaO	*Fm*-3*m*	$a = b = c$ = 4.8085 (4)	V =111.19(3)	7.17	11.72	8.62	1.70	90.5 (9)
	$Ca(OH)_2$	*P*-3*m*1	$a = b$ = 3.589 (3) c = 4.918 (5)	V = 54.9 (1)	5.30				7.9 (9)
	CeO_2	*Fm*-3*m*	$a = b = c$ = 5.4156 (2)	V = 158.84 (2)	5.84				1.6 (1)

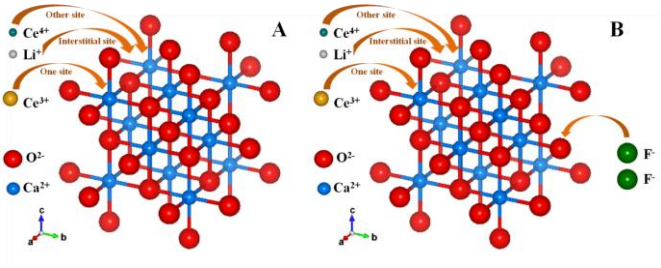

Figure 4. Schematic illustrations of doping of CaO with different ions, including (A) Ce^{3+}, Ce^{4+}, Li^+ and (B) F^-.

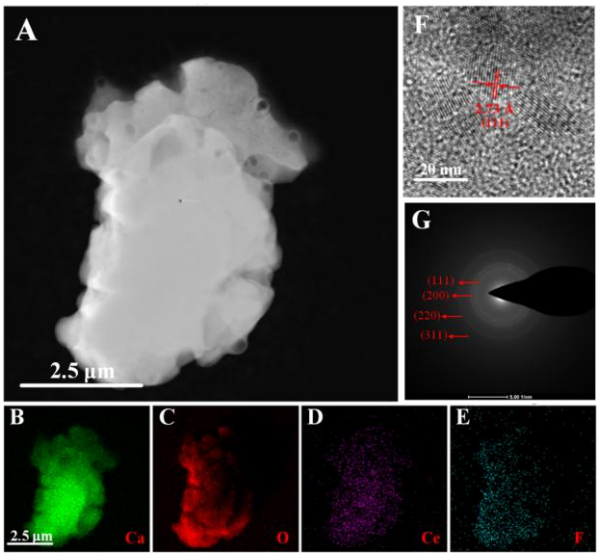

Figure 5. (A) TEM image of COCLF-6 single particle and (B-E) corresponding Ca, O, Ce and F elemental mappings. (F) HRTEM image and (G) SAED pattern of COCLF-6.

The microstructure of COCLF-6 is displayed in Figure 5. The TEM image shows that the single particle of the measured sample has an irregular shape with the size of ~3 μm (Figure 5A). Then, the elementals of Ca, O, Ce and F are distributed homogeneously in COCLF-6 single particle, further proving that the dopants, F^- in particular, have been incorporated into the CaO host lattice (Figure 5B-E). From Figure 5F and G, the spacing of the lattice fringe in the HRTEM image is 2.73 Å and the characteristic planes of CaO can well index to concentric ring patterns in the selected area electron diffraction (SAED) pattern, both of which confirm CaO phase is the dominant one in the specimen.41 Additionally, the scanning electron microscopy (SEM) image of COCLF-6 is also presented in Figure S4, showing the slight agglomerate phenomenon occurs in the as-synthesized phosphor powders.

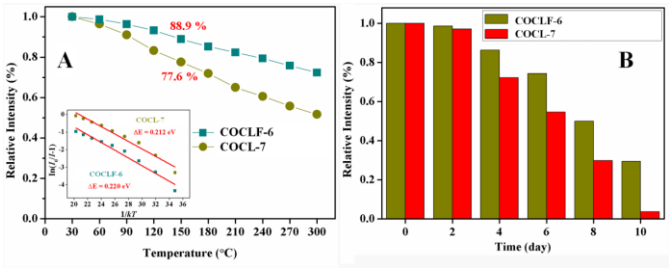

Figure 6 (A) Temperature-dependent PL intensity of COCLF-6 and COCL-7. Corresponding In(I_0/I-1) as a function of 1/kT and ΔE are shown in the inset. (B) Relative intensity as a function of time in COCLF-6 and COCL-7, exposed to air.

More importantly, a detailed comparison between COCLF-6 and COCL-7 has done and the advantage of former over latter is obtained. Firstly, the QEs of them have been measured and described by following equation

$$\eta_{QE} = \frac{\int L_s}{\int E_r - \int E_s} \quad (4)$$

where L_s presents the emission spectrum of the sample under excitation outside the integrated sphere, whereas E_r and E_s are the emission spectra obtained inside the integrated sphere under excitation without sample and the sample under excitation inside the integrated sphere, respectively. After the calculation, the QE of COCLF-6 values 66.4% excited at the wavelength of 458 nm. Under same conditions, the QE of COCL-7, which is 40.1%, shows more negative, declining by 66 %. It may be drawn a conclusion that F^- doped sample with enhanced luminescence is more conducive to the color converter. Secondly, the thermal stability improvement has been found in COCLF-6 as compared to COCL-7, as shown in the temperature-dependent PL spectra ranging from 30 to 300 °C at an interval of 30 °C (Figure 6A). With the increase of temperature, both PL intensities of samples show a descending trend, owing to the aggravation of nonradiative transfer.[42] However, the PL intensities of F^- doped and undoped samples could be separately maintained at 88.9% and 77.6% at the temperature of 150 °C, greatly catering for high-power LED application desire. Furthermore, the parameter of the activation energy (Ea) can give more information about thermal quenching behaviors of samples, and be estimated in following equation [42]

$$I(T) = \frac{I_0}{1 + A\exp\left(\frac{E_a}{kT}\right)} \quad (5)$$

where I_0 is the PL intensity at the initial temperature (30 °C), whereas $I(T)$ is the PL intensity at other measuring temperature; A and k are the constant and Boltzmann

constant, respectively. From the inset of figure 6, COCLF-6 has a smaller E_a than COCL-7, which means that the excitation process of the electrons of Ce^{3+} becomes more effectively in F^- doped sample who has lower thermal energy.[43] Being easy to react with water, CaO is instable exposed to air. To protect CaO phosphor from transforming into $Ca(OH)_2$ is crucial. Figure 6B shows the time-dependent PL intensity of COCLF-6 and COCL-7, exposed to air. After 10 days exposure, the PL intensity of COCLF-6 still hold at 29.4% while that of COCL-7 is 3.7%. That being said, F^- doping can effectively help improve the chemical stability of CaO phosphor.

For the application of high-power wLED devices, the color converter composed of the encapsulant and phosphor should have an outstanding thermal stability. Obviously, PiG technology that selects glass material as the encapsulant can be well applicable for the preparation method of the required color converter. To this end, COCLF-6 phosphor was incorporated into the red-emitting glass system with composition of SiO_2-Na_2CO_3-Al_2O_3-CaO:Eu^{3+} to form multi-color PiG with different mass ratios of phosphor to glass matrix ranging from 3:50 to 9:50. Figure 7A shows XRD patterns of host glass and COCLF-6-based PiG (mass ratio = 7:50). One broad band representing amorphous nature is found in host glass, whereas the PiG owns such amorphous hump with other diffraction peaks belonging to CaO phase. The XRD analysis results indicate that there is no phase transition of the embedded phosphor happening during the PiG preparation process. The distribution of phosphor particles inside PiG can be observed through the characterization of a confocal laser scanning microscope (CLSM) with 458 nm excitation wavelength, and the upper surface LSM image of COCLF-6-based PiG (mass ratio = 7:50) is shown in Figure 7B. The yellow highlights with some agglomerations are almost filled with whole area, demonstrating that COCLF-6 can be distributed homogeneously in glass matrix. The agglomerate phenomenon can be eliminated by applying better pulverization technology in the future.

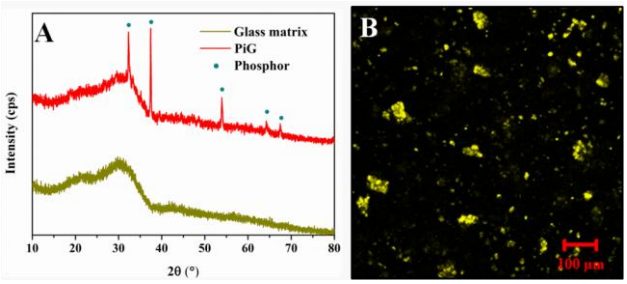

Figure 7. (A) XRD patterns of host glass and COCLF-6-based PiG (mass ratio = 7:50). (B) The upper surface LSM image of COCLF-6-based PiG (mass ratio = 7:50).

The PLE spectra of COCLF-6 and host glass are displayed in Figure 8A. The f–f transition of Eu^{3+} in host glass leads to the characteristic excitation peaks, particularly the one located at round 460 nm. Such excitation peak of host glass overlaps well with that of COCLF-6 phosphor, which could give corresponding PiG double color-emitting property excited at the same wavelength. As expected, the emission peaks of host glass originated from the transition of $^5D_0 \rightarrow {}^7F_J$ (J = 0–4) and that of phosphor, under 458 nm excitation, can be both observed in PL spectra of COCLF-6-based PiG (mass ratio = 7:50) (Figure 8B). With addition of red-emitting of Eu^{3+} provided by host glass, the PiG sample as a color converter can offer more red spectral component in the emission spectra when it is used for warm wLED application.[25] Figure 8C shows PL spectra of the PiG samples with different mass ratios of phosphor to glass matrix ranging from 3:50 to 9:50. The Ce^{3+}: 5d→4f emission intensity of PiG increases with the phosphor doping concentration, satisfying various light color demands. As seen in Figure S5A and S5B, the thermal and chemical stability of COCLF-6-based PiG have gotten great improvement compared with that of COCLF-6 phosphor. Impressively, the PL intensity of the PiG sample keeps about 90.4% after 10 days in air, signifying that COCLF-6 phosphor can be protected through PiG technology and become more satisfactory for high-power wLEDs.

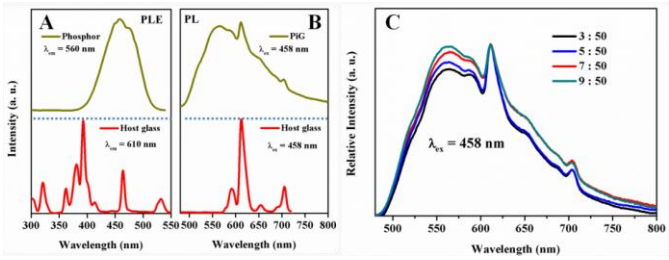

Figure 8. (A) PLE spectra of COCLF-6 and host glass. (B) PL spectra of COCLF-6-based PiG (mass ratio = 7:50) and host glass. (C) PL spectra of PiG with different mass ratios of phosphor to glass matrix ranging from 3:50 to 9:50.

PiG-based wLEDs with different mass ratios of phosphor to glass matrix ranging from 3:50 to 9:50 were fabricated by combination of the PiG samples and 460 nm high-power blue chip, and the EL spectra with 50 mA operating current are displayed in Figure 9A. The emissive component of PiG raises because of the increasing mass ratio of phosphor to glass matrix. The Commission Internationale de L'Eclairage (CIE) color coordinates and corresponding EL parameters are shown in Figure 9B and Table 2, respectively. The emitting color of the as-fabricated PiG-based wLEDs can be modified from blue white to cool white, subsequently, to warm white, and the coordinates of these wLEDs change from (0.2439, 0.1686) to (0.4036, 0.3707). Apart from the blue white one, other wLEDs show the CCT ranging from 7487 to 3364 K and LE (luminous efficacy) decreasing from 78.6 to 68.4, whereas the optimal CRI value of 82.5 is achieved in the wLED whose mass ratio is 7:50. The images of PiG (mass ratio = 7:50)-based wLEDs out operation and in operation are also supplied in the inset of Figure 9B. Above results demonstrate that the obtained PiG-based wLEDs, especially the one with high CRI, can be better applied in indoor illumination.

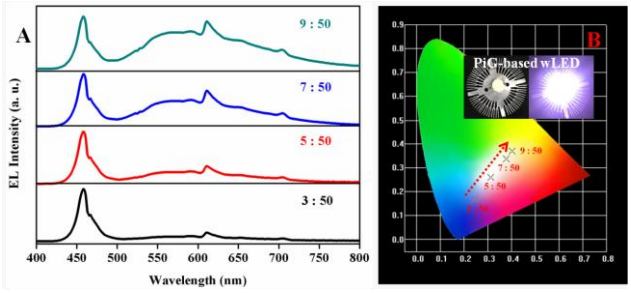

Figure 9. (A) EL spectra and (B) CIE color coordinates of PiG-based wLEDs with different mass ratios of phosphor to glass matrix ranging from 3:50 to 9:50 with 50 mA operating current. The insets of (B) show images of PiG (mass ratio = 7:50)-based wLEDs out operation and in operation.

Table 2. EL parameters of PiG-based wLEDs with different mass ratios of phosphor to glass matrix ranging from 3:50 to 9:50.

mass ratio	x	y	CCT (K)	Ra	LE (lm/w)
3:50	0.2439	0.1686	-	-	-
5:50	0.3137	0.2605	7487	73.9	78.6
7:50	0.3769	0.3386	3774	82.5	73.1
9:50	0.4036	0.3707	3364	76.6	68.4

Figure 10 shows EL spectra of PiG (mass ratio = 7:50)-based wLEDs under different operating currents (50-300 mA). With the increase of the operating current, the EL intensity of the fabricated wLED device has been enhanced. However, corresponding

coordinates shifts from (0.3769, 0.3386) to (0.3629, 0.3101), the value of CCT increases from 3374 to 4186 K and the value of CRI also raises from 82.5 to 84.1. The variations of them are a little bit large, but within acceptable limits.[44] Such situation can be attributed by the reduced intensity of the emissive component of PiG along with the operating current, as seen in Figure S6. The overall QE of PiG is slightly deficient, causing the PiG sample can not be excited by the high-power blue chip, adequately. The above problem existed in PiG-based wLEDs is hopeful to be solved through obtaining high QEs of CaO:Ce^{3+}, Li^+, F^- phosphor and the red-emitting host glass in the future. On the whole, the as-prepared PiG-based w-LEDs have acceptable color stability at various driving currents.

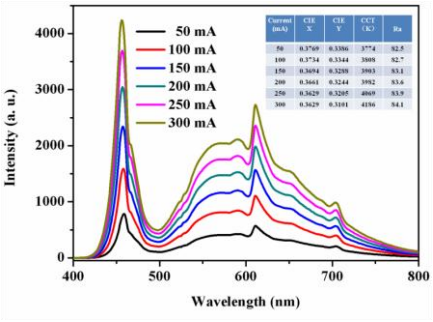

Figure 10. EL spectra of PiG (mass ratio = 7:50)-based wLEDs under different operating currents (50-300 mA). Corresponding parameters are shown in the inset.

4. Conclusions

In summary, CaO:Ce^{3+}, Li^+, F^- phosphors using CeF_3 and LiF as the cerium, lithium and fluorine sources have been prepared by high temperature solid-state reaction. The structure and luminescence as well as the stability of them were investigated in detail. As a result, CaO:Ce^{3+}, Li^+, F^- has more red component in their emission spectrum than YAG:Ce^{3+}. Notably, the critical doping concentration of Ce^{3+} in CaO:Ce^{3+}, Li^+, F^- phosphors reaching 0.06 % is just a tenth of that of F^- undoped samples, and accounts for stronger luminescence. F^- doping can effectively remove the impurity of CeO_2 which could influence the luminescent intensity of phosphor. Furthermore, the representative COCLF-6 sample shows a better QE of 66.4% and more excellent thermal and chemical stability compared with COCL-7. In order to acquire improved properties, COCLF-6 phosphor was introduced into the red-emitting glass system with composition of SiO_2-Na_2CO_3-Al_2O_3-CaO:Eu^{3+} to fabricate various PiG. The as-obtained PiG with better performance shows great potential for high-power wLEDs, and the optimal PiG-based wLED owns color coordinates of (0.3769, 0.3386), a CCT of 3774 K, a CRI of 82.5 and a LE of 73.1 when the mass ratio of phosphor to glass matrix is 7:50 in PiG. Besides, such PiG-based wLED also shows acceptable color stability under different drive currents. Generally, CaO:Ce^{3+}, Li^+, F^- can be expected to be an alternative yellow phosphor for blue-emitting excited warm wLEDs, especially for high-power ones.

Conflicts of interest

There are no conflicts to declare.

Acknowledgements

The present work was supported by the National Natural Science Foundation of China (Grant No. 21671070), the Project for Construction of High-level University in Guangdong Province, the Teamwork Projects funded by the Guangdong Natural Science Foundation (Grant No. S2013030012842), the Guangzhou Science & Technology Project (No. 201704030086) and the Open Project Fund from Key Laboratory of Advanced of Materials of Yunnan Province (No. 2018KF01).

Notes and references

1. J. Meyer and F. Tappe, *Adv. Opt. Mater.* **2014**, *3*, 424-430.
2. J. Cho, J. H. Park, J. K. Kim and E. F. Schubert, *Laser Photonics Rev.* **2017**, *11*, 1600147.
3. J. Li, J. Yan, D. Wen, W. U. Khan, J. Shi, M. Wu, Q. Su and P. A. Tanner, *J. Mater. Chem. C* **2016**, *4*, 8611-8623.
4. Z. Xia and A. Meijerink, *Chem. Soc. Rev.* **2017**, *46*, 275-299.
5. H. Chen, H. Lin, J. Xu, B. Wang, Z. Lin, J. Zhou and Y Wang, *J. Mater. Chem. C* **2015**, *3*, 8080-8089.
6. J.-J. Shyu and C.-W. Yang, *Mater. Chem. Phys.* **2017**, *193*, 339-347.
7. Y. Tang, S. Zhou, X. Yi, S. Zhang, D. Hao and X. Shao, *J. Am. Ceram. Soc.* **2017**, *100*, 2590-2595.
8. Y. Wu, Z. Chi and T. He, *J. Mater. Sci: Mater. Electron* **2017**, *28*, 14591-14595.
9. K. Bartosiewicz, V. Babin, J. A. Mares, A. Beitlerova, Y. Zorenko, A. Iskaliyeva, V. Gorbenko, Z. Bryknar and M. Nikl, *J. Lumin.* **2017**, *188*, 60-66.
10. C.-e. Huang, X. Lu, M. Lu, and Y. Huan, *Ceram. Int.* **2017**, *43*, 10624-10627.
11. S.M. Salman, S.N. Salama and H.A. Abo-Mosallam, *Ceram. Int.* **2017**, *43*, 9424-9430.
12. P.-L. Boey, G. P. Maniam and S. A. Hamid, *Chem. Eng. J.* **2011**, *168*, 15-22.
13. W. Lehmann, *J. Lumin.* **1973**, *6*, 455-470.
14. A. Yousif, R. E. Kroon, E. Coetsee, O. M. Ntwaeaborwa, H. A. A. Seed Ahmed and H. C. Swart, *Appl. Surf. Sci.* **2015**, *356*, 1064-1069.
15. D. Prakash and K. R. Nagabhushana, *Nucl. Instrum. Methods Phys. Res. B* **2016**, *379*, 136-140.
16. Y. Jin, Y. Hu, L. Chen, X. Wang, G. Ju, Z. Mou and F. Liang, *Opt. Commun.* **2013**, *311*, 266-269.
17. L. Feng, Z. Hao, X. Zhang, L. Zhang, G. Pan, Y. Luo, L. Zhang, H. Zhao and J. Zhang, *Dalton Trans.* **2016**, *45*, 1539-1545.
18. Q. Liu, H. Yin, T. Liu, C. Wang, R. Liu, W. Lü and H. You, *J. Lumin.* **2016**, *177*, 349-353.
19. Z. Hao, X. Zhang, Y. Luo, L. Zhang, H. Zhao and J. Zhang, *J. Lumin.* **2013**, *140*, 78-81.
20. Z. Hao, X. Zhang, X. Wang and J. Zhang, *Mater. Lett.* **2012**, *68*, 443-445.
21. D. Chen, W. Xiang, X. Liang, J. Zhong, H. Yu, M. Ding, H. Lu and Z. Ji, *J. Eur. Ceram. Soc.* **2015**, *35*, 859-569.
22. Y. K. Lee, J. S. Lee, J. Heo, W. B. Im and W. J. Chung, *Opt. Lett.* **2012,** *37*, 3276-3278.
23. R. Zhang, H. Lin, Y. Yu, D. Chen, J. Xu and Y. Wang, *Laser Photonics Rev.* **2014**, *8*, 158-164.
24. X. Zhang, J. Yu, J. Wang, C. Zhu, J. Zhang, R. Zou, B. Lei, Y. Liu and M. Wu, *ACS Appl. Mater. Interfaces* **2015**, *7*, 28122-28127.
25. J. Zhong, D. Chen, Y. Zhou, Z. Wan, M. Ding, W. Bai and Z. Jia, *Dalton Trans.* **2016**, *45*, 4762-4770.
26. F. Iqbal, S. Kim, H. Kim, *Opt. Mater.* **2017**, *72*, 323-329.
27. J. Zhong, W. Xu, Q. Chen, S. Yuan, Z. Ji and D. Chen, *Dalton Trans.* **2017**, *46*, 9959-9968.
28. X. Zhang, J. Yu, J. Wang, B. Lei, Y. Liu, Y. Cho, R.-J. Xie, H.-W. Zhang, Y. Li, Z. Tian, Y. Li and Q. Su, *ACS Photonics* **2017**, 4, 986-995.
29. Q.-Q. Zhu, X. Xu, L. Wang, Z.-F. Tian, Y.-Z. Xu, N. Hirosaki and R.-J. Xie, *J. Alloys Compd.* **2017**, *702*, 193-198.
30. S. Yi, W. J. Chung and J. Heo, *J. Am. Ceram. Soc.* **2017**, *100*, 2378-2381.
31. H.-A. Park, Y. K. Lee, W. B. Im, J. Heo and W. J. Chung, *Opt. Mater.* **2015**, *41*, 67-70.
32. J. Deng, W. Li, H. Zhang, Y. Liu, B. Lei, H. Zhang, L. Liu, X Bai, H. Luo, H. Liu, W.-R. Liu and J. Wang, *Adv. Opt. Mater.* **2017**, *5*, 1600910.
33. S.-P. Lee, C.-H. Huang, T.-S. Chan and T.-M. Chen, *ACS Appl. Mater. Interfaces* **2014**, *6*, 7260-7267.

34. H. Li, R. Zhao, Y. Jia, W. Sun, J. Fu, L. Jiang, S. Zhang, R. Pang and C. Li, *ACS Appl. Mater. Interfaces* **2014**, *6*, 3163-3169.
35. *TOPAS V4.2: General profile and structure analysis software for powder diffraction data−User's Manual*, Bruker AXS, Karlsruhe, Germany. 2008.
36. W. Primak, H. Kaufman and R. Ward, *J. Am. Chem. Soc.* **1948**, *70*, 2043-2046.
37. H. E. Petch, *Acta Crystallogr.* **1961**, *14*, 950-957.
38. M. Yashima and S. Kobayashi, *Appl. Phys. Lett.* **2004**, *84*, 526-528.
39. Z. Wang, J. Zou, Y. Li, C. Zhang, M. Shi, B. Yang, H. Zhou, Y. Liu and N. Liu, *J Mater. Sci: Mater. Electron* **2017**, *28*, 16633-16638.
40. X. Liu, F. Wu, S. Chen, M. Gu, H. Chen, B. Liu, S. Huang and J. Zhang, *J. Lumin.* **2015**, *161*, 422-425.
41. E. Song, J. Wang, S. Ye, X.-B. Yang, M. Peng, Q. Zhang and L. Wondraczek, *Adv. Opt. Mater.* **2017**, *5*, 1700070.
42. R.-J. Xie, N. Hirosaki, N. Kimura, K. Sakuma and M. Mitomo, *Appl. Phys. Lett.* **2007**, *90*, 191101-191103.
43. Y.-C. Wu, D.-Y. Wang, T.-M. Chen, C.-S. Lee, K.-J. Chen and H.-C. Kuo, *ACS Appl. Mater. Interfaces* **2011**, *3*, 3195-3199.
44. Y. H. Kim, P. Arunkumar and W. B. Im, *Ceram. Int.* **2015**, *41*, 5200-5204.